Journal of Air Transport Management 107 (2023) 102356

Contents lists available at ScienceDirect

Journal of Air Transport Management

journal homepage: www.elsevier.com/locate/jairtraman

3D-flight route optimization for air-taxis in urban areas with Evolutionary Algorithms and GIS

Moritz Hildemann [a,*], Judith A. Verstegen [b]

[a] University of Münster, Institute for Geoinformatics, Heisenbergstraße 2, 48149 Münster, Germany
[b] Utrecht University, Department of Human Geography and Spatial Planning, Heidelberglaan 8, 3584 CS Utrecht, The Netherlands

ARTICLE INFO

Keywords:
Urban air management
Flight route optimization
Genetic Algorithms
GIS
Air-taxis

ABSTRACT

Electric aviation is being developed as a new mode of transportation for the urban areas of the future. This requires urban air space management that considers these aircraft. Flight routes need to be determined that avoid no-fly areas, and minimize flight time, energy consumption and added noise. Yet, no method currently exists for optimizing urban flight routes under multiple conflicting objectives while avoiding three-dimensional restricted areas. In our work, this research gap is overcome by optimizing 3D-routes with the multi-criteria optimization technique called Non-dominated Sorting Genetic Algorithm II. We propose a novel procedure in the optimization process to incorporate geographical representations. Furthermore, we include a seeding procedure for initializing the flight routes and repair methods for invalid flight routes that may arise during the optimization process. We apply the optimization to a case study in Manhattan (New York City) for two different aircraft types, the Lilium Jet (vectored thrust) and the EHANG 184 (wingless multicoptor), under three objectives concerning flight time, energy consumption and added noise. Compared to a least-distance path, flight routes were obtained with maximum improvements of 38% in added noise, 65% in flight time and 52% in energy consumption for the EHANG 184. For the Lilium jet, maximum improvements of 43% in added noise, 47% in flight time and 47% in energy consumption were obtained. Still, the obtained noise addition levels by the aircraft in New York City exceed 5 dB, which is considered as long-term noise annoyance. We illustrated that minimizing the added noise requires high search effort compared to the other two objectives. Upon further analysis of the optimization results, we conclude that the Lilium jet as representative of the eVTOL type vectored thrust is more sensitive to flight route changes than the multicoptor EHANG 184. This information may help in air taxi type choice for a certain region as well as in flight route planning.

1. Introduction

The traffic in today's Megacities is congested and the commuting times in these cities are high. Therefore, a new mode of transport has been developed during the past years: The air taxi type Electrical Vertical Take-Off and Landing vehicles (eVTOL). The expected potential demand in the highly competitive air taxi market in the United States only is already 80.000 passengers per day Goyal (2018), and Rajendran and Srinivas (2020) expect air taxi operations in urban space within the forthcoming years. Electrical Vertical Take-Off and Landing vehicles are air taxis with suitable flight characteristics for the urban air space: Vertical landing and take-off allows precise manoeuvring, and the electric propulsion makes them quieter, safer, and less expensive to operate compared to non-electrical helicopters (Garrow et al., 2021). In order to successfully integrate eVTOL into the urban air space, flight laws, other airspace users, and citizens have to be respected (Bauranov and Rakas, 2021). Air space segmentation into fly and no-fly zones, depending on the location and the time of the day (Geister, 2017), can ensure permanently secured locations of special safety concern like hospitals as well as occasional no-fly zones in severe weather conditions or during public assemblages.

After segmenting the air space, flight routes for the eVTOL need to be formulated. However, the optimality of a route depends on the viewer's perception. For eVTOL operator, the commuting time and the energy cost for the flight route might be crucial. For the commuter, the safety, commuting time and price might be the most relevant criteria (Baur et al., 2018), whereas for the other citizens, the discomfort produced by the aircraft noise might be the most important criterion (Berglund et al., 1999). Therefore, a method is demanded that incorporates multiple objectives linked to spatially-varying attributes in the search for optimal flight routes within the fly zones.

* Corresponding author.
E-mail addresses: jhildema@uni-muenster.de (M. Hildemann), j.a.verstegen@uu.nl (J.A. Verstegen).

https://doi.org/10.1016/j.jairtraman.2022.102356
Received 30 June 2020; Received in revised form 29 December 2022; Accepted 29 December 2022
Available online 12 January 2023

Geographical Information Systems (GIS) enable to compute cost-surfaces based on weighted spatial attributes within fly zones (Hildemann and Delgado, 2019). With such a cost surface, the least cost path between an origin and a destination can be found (Durmaz et al., 2019). In that case, the altitude is included in the cost value at each grid cell of the cost surface. The outcome is a two-dimensional line with each node extracted to the minimal flight height surface. Another GIS method is 3D-Routing along 3D-Networks. This solves the combinatorial problem to travel along an existing network (Atila et al., 2013), which can be designed to avoid restricted airspace (Dai and Low, 2022). On street networks, the possible solutions are limited by the existing streets. The problem of the cost-surface method is that the weights of the objectives have to be predefined. Furthermore, both methods have the drawback that they do not search the full 3D-space. The cost-surface method only finds routes on the minimal height surface, while the 3D routing methods finds routes in a predefined 3D network. This is a shortcoming in the context of eVTOL because those aircraft can move in space without being bound to a surface or network.

This work aims to fill the stated research gap to optimize routes for eVTOL transportation in 3D fly zones with multiple objectives. Borrowing techniques that have been applied to other domains, such as pipe routing (Sandurkar and Chen, 1999) and drone mission planning (Peng et al., 2011), we use a hybrid of GIS and Evolutionary Algorithms, a set of search techniques for continuous optimization (Sivanandam and Deepa, 2008). The generalizable method is applied to a study case of urban eVTOL routing in Manhattan (New York City). The routes are evaluated for three different criteria, specific for the 3D-routing in eVTOL transportation given the different stakeholders mentioned above: The total flight time in minutes, the total energy consumption in kilowatt per hour and the additional (to already existing background noise) noise pollution in decibels. Our research questions are (1) Can the three objectives be optimized while complying with the air space restrictions and noise regulations? If yes, how much can a least-distance route computed with a GIS be improved for the objectives in the highly restricted air space of New York City for two different eVTOL? and (2) What information for air space management can be derived from the study case results?

2. Background

Air taxis are expected to be introduced in the urban air space in the future (Ahmed et al., 2021). From a limited competition of air taxis to medium-ranged rail commuting in year 2018 (Sun et al., 2018), the new eVTOL air taxis with different flight characteristics could expand the market to shorter distances, competing with other means of transport. Rajendran and Srinivas (2020) expect air taxi operations in urban space within the forthcoming years and identify multiple actions that need to be taken for realizing air taxi operations, e.g. ride-matching, pricing strategies, vehicle maintenance scheduling, and pilot training and recruitment.

Ahmed et al. (2021) analyse the willingness of citizens to use and pay for air taxi operations. Their survey analysis shows that respondents show the willingness to use and pay for such services if they expect benefits. Expected benefits are decreased commuting times and fewer and less severe crashes compared to ground transportation options. They advise decision-makers to focus on developing regulatory frameworks that increase safety in air taxi operations. Ward et al. (2021) analyse the willingness of passengers to fly in autonomous air taxis. They found that introducing new vehicles without strong safety records reduces the willingness. Ahmed et al. (2021) and Ward et al. (2021) reflect on the willingness of citizens to use and pay for air taxis, but citizens not actively using the new mode of transport need to be considered as well.

Citizens at ground prefer not to be exposed to additional risk or noise by urban air taxi operations (McKinsey & Company, 2021). Despite declining accident rates (Budde et al., 2021), the number of accidents will likely increase when the use of air taxis within the dense urban air space is intensified. Besides, urban air mobility increases the already high noise levels in cities by up to 40 dB at the ports, as results from Glaab et al. (2019) indicate. de Paiva Vianna et al. (2015) show that exposure to high noise levels has a significant effect on the annoyance and sleep quality of affected people, and the Environmental Protection Agency (1974) defines high noise levels as pollutant. The implementation of no-fly zones at the right locations may help to reduce the risk and annoyance to a minimum and hence to increase the likelihood of acceptance. Geister (2017) propose a concept for no-fly zones, and Hildemann and Delgado (2019) proposed an implementation of such three-dimensional no-fly zones in urban air space. The air space restrictions consider both flight regulations and a subset of land uses and points of interest like parks, schools or recreational areas.

In addition to restricting specific areas of the urban air space, flight route planning plays an important role to reduce negative side effects (Rajendran and Pagel, 2020). Many trajectory concepts were proposed that reduce the flight time, e.g. Zhao et al. (2020), and some include additional aspects like emissions (Okuniek et al., 2016), manoeuvrability aspects (Wang et al., 2021), or wind (Pradeep et al., 2022). Pradeep et al. (2020) state that wind has little impact on short flights in urban air space. Even though noise reduction for urban air mobility is identified as an important goal by researchers (Eißfeldt, 2020) and by space agencies (Rizzi et al., 2020), it has not been incorporated in planning flight routes so far.

3. Methods

3.1. Overview

The workflow of the used methods to optimize flight routes is displayed in Fig. 1. The flight routes, individuals represented as 3D point arrays and 3D lines, are randomly initialized in a 3D channel (Section 3.6.1). After creation, they are validated and repaired in order to be conform with flight regulations (Section 3.6.2). All valid flight routes are evaluated for the three objectives shortest flight time, least energy consumption and least added noise, and are given a non-domination rank (Section 3.6.3). Individuals are selected based on their non-domination rank in order to produce children: the 3D points of the parents are combined and mutated with the aim of producing a better flight route (Section 3.6.4). The children are validated and repaired, and the best flight routes from the parent and children generation combined form the next generation (Section 3.6.5).

In the next sections, the concept of evolutionary algorithms (Section 3.2), the case study (Section 3.3), the used air-taxi representatives (Section 3.4) and the objective functions (Section 3.5) are explained first. After that, each step in our proposed optimization approach (Fig. 1) is described in detail in Section 3.6.

3.2. Evolutionary algorithm

The principle of evolutionary algorithms mimics the biological evolution of cells, organs, individuals and populations (Sivanandam and Deepa, 2008). The Darwinian theory of natural selection proposes that organisms that are fitter than other organisms have a higher probability to survive and thus to pass on the genes in reproduction processes. Evolutionary algorithms mimic this idea by analysing a population consisting of several potential solutions to a given problem (Sivanandam and Deepa, 2008). The evolutionary algorithm detects the individuals with the highest fitness within this population, in other words the currently best solutions for to problem (Holland, 1975). These individuals have a higher probability of being selected for reproduction (selection process). In the reproduction, the crossover process determines how elements of the parents are recombined to produce a child. In contrast, the mutation process generates characteristics that are not inherited by the parents by randomly perturbing elements (Holland, 1975). The

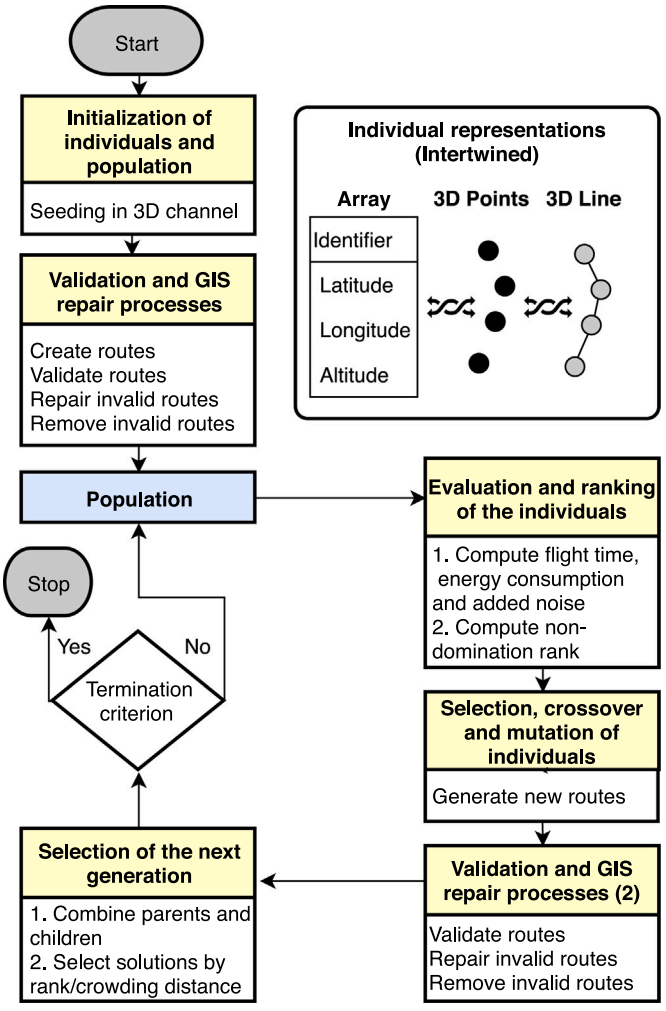

Fig. 1. Optimization process flowchart.

next generation, consisting of old (parents) and new (children) individuals, is expected to have a higher fitness. The algorithm runs until it reaches a predetermined termination criterion. The evolutionary algorithm searches for so called non-dominated solutions. Non-dominated solutions are optimal compromises between the objectives (Sivanandam and Deepa, 2008), i.e. solutions that cannot be improved for one objective without becoming worse for the other two objectives (Reddy and Kumar, 2015). All non-dominated solutions can be plotted together to form a so-called Pareto front. Each point on the Pareto front is optimal, but the "importance" or weight of the objectives varies for each point. As such, the Pareto front visualizes trade-offs between the objectives.

In our study, we use an evolutionary algorithm to produce valid optimal flight routes for the objectives shortest flight time, lowest energy consumption and minimal added noise level (Fig. 1). In this study, the Non-Dominated Sorting Genetic Algorithm II (NSGA II) developed by Deb et al. (2002) is used as evolutionary algorithm strategy. This strategy allows to find multiple pareto-optimal solutions in one simulation run. It is well known in the field of optimization and the details are outlaid by its developers.

3.3. Case study and reference route

The urban area of Manhattan, New York City, (Fig. 2) is an often used study area for air taxi marketing (Lilium Aviation, 2019) and air taxi market studies (Goyal, 2018), as the traffic is congested and the city yields one of the highest market potentials (Goyal, 2018). Moreover, most of the air space is likely to be regulated into fly and no-fly zones, where the latter can be divided into restricted and protected air space (Fig. 2).

Table 1
Vertical and horizontal restrictions in meters.

Landuse	Vertical restriction	Horizontal restriction
Airport	600	7620
Hospitals	300	300
Universities	200	300
Parks	300	100
Graveyards	300	100
Recreational Areas	300	100
Rooftops	152.4	–

- Restricted air space due to flight regulations. Areas around airports within the horizontal distance of 25.000 ft (7620 m) belong to this category, as well as the space below the height of 500 ft (152.4 m) and above the height of 700 ft (213.36 m) measured from the rooftops (Federal Aviation Administration, 2017).
- Protected airspace to consider the possible negative side effects to the citizens (Geister, 2017). Flying above these specified land uses can lead to annoyance or discomfort: examples are schools, graveyards, recreational areas.

We assume that the vertical and horizontal minimum distance to be maintained by aircraft depends on the land use (Table 1), which is retrieved from OpenStreetMap (OpenStreetMap contributors, 2019). Furthermore flight obstacle maps from Federal Flight Administration (2016) and rooftop heights from Open Data NYC (2018) are obtained.

To assess the performance of the method described in the next sections, i.e. as a reference route, a least-cost path on the minimal flight height plane, where the cost is the accumulated euclidean distance along all raster cells. The least cost flight route from Hildemann and Delgado (2019) was chosen as reference route, which is ≈6 kilometres long (Fig. 2).

3.4. Selected eVTOL

Many eVTOL configurations exist with different thrust types, among of them "Thrust, Lift and Cruise, Wingless, Hover Bikes and Personal Flying Devices, Electric Helicopters" (Electric VTOL News, 2019). The flight characteristics of the aircraft have an impact on the objective values and thereby on the optimal flight routes. Therefore, in our case study, the wingless multicoptor eVTOL EHANG 184 (EHANG, 2019) is compared to the vectored thrust eVTOL Lilium Jet (Lilium Aviation, 2019). We chose these two because they were found to vary the most in short-distance and long-distance performance (Bacchini and Cestino, 2019). The wingless multicoptor is more energy efficient in short distance missions, whereas the Lilium Jet is more energy efficient and faster in long-distance missions. We obtained the aircraft parameter values needed to calculate the energy consumption and speed from Bacchini and Cestino (2019) (Table 2).

3.5. Objectives for flight route optimization

3.5.1. Flight time

The first objective is to minimize flight time. To compute the flight time, the maximum flight speed at any position of the flight route needs to be known. The maximum flight speed is limited by three different factors: The maximum allowed flight speed by the flight authorities, the maximum possible flight speed by the aircraft and the maximum flight speed that is still comfortable for the passenger given the flight manoeuvre. The maximum cruise speed for the Lilium Jet is 252 km/h, whereas the EHANG 184 is slower with a maximum speed of 100

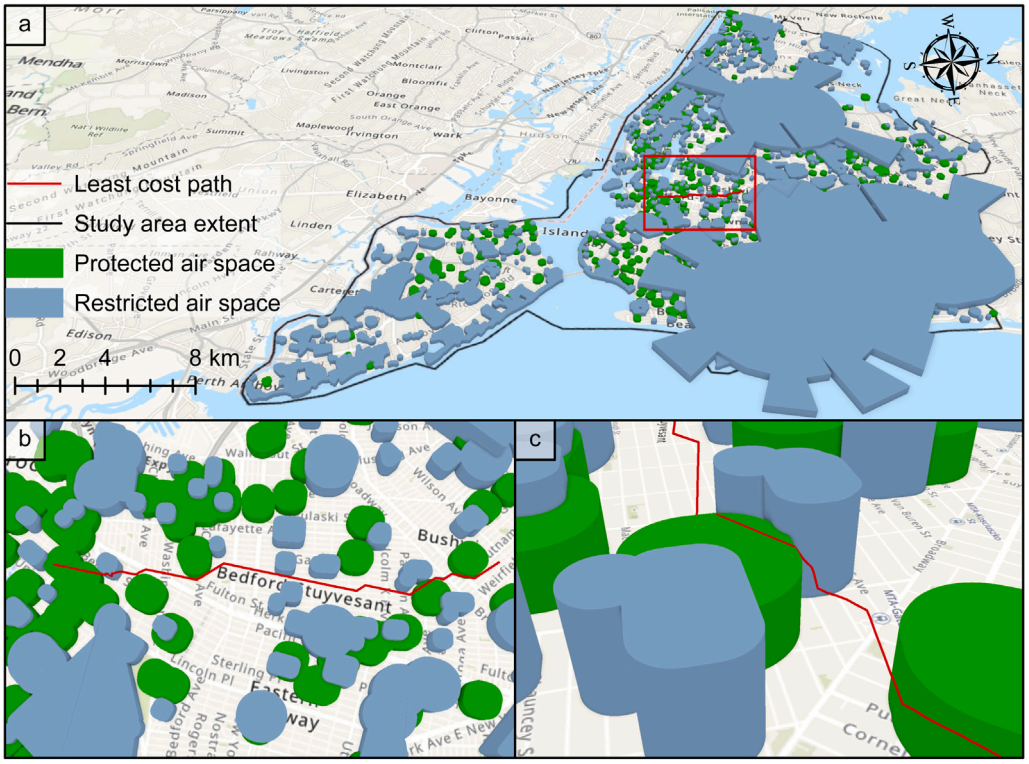

Fig. 2. Maps of the study area New York City: (a) Overview of the study are with the protected and restricted air space, (b) Overview of the least cost path to be optimized, (c) Detail view of least cost path.

km/h (Bacchini and Cestino, 2019). We assume, that the flight agencies limit the maximum velocity to 100 km/h. To guarantee flight comfort, a maximum gravitational force equivalent (g_{Force}) of 1.25 is aimed for. The formulas for the calculation are provided in Appendices B.1 and B.2.

3.5.2. Energy consumption

The second objective is to minimize energy consumption. With the variables flight velocity and the flight angle, the required power can be calculated for each flight route segment, when the aircraft flight characteristics are known (Table 2). These flight characteristics change per aircraft type, therefore the energy consumption is aircraft-dependent. The vectored thrust aircraft can generate more lift with increasing flight velocity with their wings. The wingless multicoptor generates less additional lift (Sadraey, 2009). As aircraft with wings have a better lift/drag ratio with increasing flight speeds, the energy consumption is speed dependent for the Lilium. The multicoptor from EHANG on the other hand has no wings and can only produce lift with its rotors. The required energy for landing, hovering, acceleration and deceleration are constant (Table 2). The formulas for the calculation are provided in Appendix B.3.

3.5.3. Added noise

The last objective is to minimize the noise added to the existing background noise at the ground. The Environmental Protection Agency (1974) and the World Health Organisation (Berglund et al., 1999) support the approach of planning flight routes above areas with high noise levels. This leads to less added noise in quiet residential areas.

We compute the added noise perpendicular from the aircraft to the surface. First, the sound pressure arriving at the ground is calculated with the noise emission of the aircraft (Kinsler, 2000). As the noise emission values are not made public by the aircraft manufacturers, the target noise levels of Uber Elevate (2016) are used. Their goal is a maximum of "62 dB at 500 ft altitude". This translates to a noise pressure of 100 dB in a reference distance of one meter. Using the flight height of the aircraft and the noise pressure of 100 dB, we get the perceived noise level at ground from the aircraft. Next, we combine the noise emission of the aircraft with the background noise at the ground, to compute the added noise. The formulas for the calculation are provided in Appendix B.4.

Table 2
Aircraft parameters for calculation of energy consumption from Bacchini and Cestino (2019). Cruise power variable for the Vectored Thrust eVTOL: 28 kW in optimal flight speed, 36 kW at 100 km/h, variable (x) below 100 km/h flight speed. C_L in drag polar is the lift coefficient of the aircraft wings.

	E-Hang 184	Lilium
eVTOL type	Wingless Multicoptor	Vectored Thrust
Cruise power in kW	34.6	28/36/x
Hover power in kW	42.7	187
Acceleration energy in kW	42.7	187
Deceleration energy in kW	42.7	187
Acceleration speed in $\frac{m}{s^2}$	2	2
Deceleration speed in $\frac{m}{s^2}$	−2	−2
Wing area in m^2	0	3.6
Empty weight in kg	168	490
Drag polar	–	$0.0163 + 0.058C_L^2$

3.6. Optimization with Genetic Algorithms and GIS

3.6.1. Initialization of individuals and population

One individual is one 3D-flight route and all individuals together form the population. The representation of the individuals is a sequence of georeferenced 3D-points (Fig. 1). Each point consists of the x and y coordinates and the height above the ground in meters. Additionally, each route consists of a smoothed line that connects the 3D-points (Fig. 1). The line is needed to validate a route because straight connections between the points can intersect with the restricted air space, even if the points are positioned outside of the restricted air space. The array representation, the 3D-points and the 3D-line are intertwined (Fig. 1). If

one of these three representations of one individual changes, the other two representations are updated accordingly.

The initial population is formed using a seeding approach (Friedrich and Wagner, 2015). That means that prior knowledge of the problem and its solutions exists and is used for generating the initial population for an evolutionary algorithm. Seeding is considered especially useful when the initialization and evaluation of the solutions are expensive (Friedrich and Wagner, 2015). If we would make the initial population completely random, a very large part of the population would not connect start and end point, be very long, and insect with the restricted airspace. Therefore, we use the existing knowledge of the least-cost path (Section 3.2, Fig. 2), as that path is known to efficiently connect the start and end point and does not interfere with the restricted airspace. The initial population is formed by individuals randomly created within an 1800-meter-wide 3D channel around the least-cost path. The height of the channel depends on the distance from the minimal height to the maximal height at each position. If a point is created in the restricted airspace, the point is deleted. The initialization of individuals is repeated until the population size of 16 is reached.

3.6.2. Validation and GIS repair processes

An individual is invalid when it violates one of the defined constraints. In our case, the following conditions need to be fulfilled for an individual to be valid: (1) No 3D-line segment intersects with the minimal flight height plane, and (2) No 3D-line segment intersects with the restricted and protected airspace.

The covered area of restricted and protected airspace is ≈ 41% of the study area, and the flight route is ≈19 kilometres long. In case of a constraint violation at any point of the optimization, it is inefficient to discard the individual, because the computation effort for producing a solution is high and the probability of violating a constraint is high. Therefore, we first try to 'repair' the individual. A 3D point is relocated when it is inside a restricted or protected air space. When a line interferes with a restricted or protected air space, we add points to make the line circumvent the restricted or protected air space (see Appendix A for more details). If the individual is still invalid after a repair trial, it is removed.

3.6.3. Evaluation and ranking of the individuals

All valid individuals are evaluated by applying the objective functions for the flight time, the energy consumption and the noise addition. As such, each individual is assigned three values that express its quality. These values are used to compute a non-domination rank, which was introduced and explained by Deb et al. (2002). All solutions not dominated by any other solution are assigned the first rank. The second rank is assigned to solutions that are not dominated by any solution not belonging to the first rank. This process continues until every solution got assigned a non-domination rank.

3.6.4. Selection, crossover and mutation of individuals

The selection of the individuals for the crossover and mutation operations is done with a tournament selection (Sivanandam and Deepa, 2008). From the population, a subset of four solutions is randomly selected, the Tournament Group. From the Tournament Group, the individual with the lowest non-domination rank (i.e., the best score) wins (Deb et al., 2002). If two solutions have the same non-domination rank, an additional metric is used to choose the superior solution, the crowding distance. The crowding distance is the distance to neighbouring points in the objective space (Deb et al., 2002). The solution with the highest crowding distance wins to maintain the maximum diversity in the population. The *Tournament Winner* proceeds to the crossover and mutation.

For the crossover, the genes of two *Tournament Winners* from the selection process are combined with a k-point crossover (Sivanandam and Deepa, 2008). The produced children inherit the combined elements of the parents. In our approach, the number of points can differ per solution, so the crossover algorithm is slightly adapted (see Appendix C). The used mutation technique for the optimization of 3D-flight routes bases on the idea of Peng et al. (2011). They split a mutation process into deletion, insertion and disturbance of points. These processes were slightly adapted to increase the probability of generating valid solutions: The insertion and deletion of points is done deterministically instead of randomly. For the insertion, points are sought with the highest distance to the neighbouring points. For the deletion, points are sought with the lowest distance to the neighbouring points. The reason for this approach is the high proportion of restricted airspace. Higher distances between the points increase the probability of a line intersecting with the restricted and protected airspace, which makes a route invalid.

3.6.5. Selection of the next generation

After producing and evaluating the children in every generation, the non-domination rank and the crowding distance are reused for selecting the individuals that form the next generation. In the NSGA II, the individuals that replace the old population are selected from the parents and children. The solutions with the best ranks are selected until the population size of 16 is reached again. By doing test of convergence, we selected a number of 20 produced generations as the termination criterion to stop the optimization.

3.6.6. Data and software availability

In this project, the Python libraries of the licensed GIS desktop application ArcGIS Pro 2.4.1[1] are used for processing and storing the spatial data. The optimization algorithm is developed in Python 3.68.[2] The repository containing the optimization implementation (Hildemann, 2020) and the required spatial data (Hildemann and Delgado, 2020) are permanently available at Mendeley Data.

4. Results

4.1. The extremes of the Pareto front

The flight routes at the Pareto front of the Lilium jet have a flight time between 221 and 261 s, an energy consumption between 13.4 and 30.6 kWh, and added noise between 3.61 and 4.56 dB (Fig. 3). On the other hand, the flight routes at the Pareto front of the EHANG 184 have a flight time between 222 and 254 s, an energy consumption between 3.76 and 6.73 kWh, and added noise between 3.62 and 4.77 dB. The extremes of the Pareto front (red, blue and green dot in Fig. 3), represent the solutions with all weight on a single objective, i.e. the route with the shortest flight time, the route with the lowest energy consumption and the route with the lowest added noise. These three routes are found to resemble each other closely at the start and end point of the route for both the EHANG 184 (Fig. 4a) and the Lilium (Fig. 4b). In the middle of the route, with several scattered restricted or protected air spaces, the differences are larger. For both eVTOL types, the route with the shortest flight time goes through a corridor between two small restricted air spaces, while both least-energy routes bypass the two restricted or protected airspaces on the western side. The routes with the least added noise have in common that they are composed of long route segments arranged in parallel with the main street on the north western area of the map, because the added noise from the aircraft is lower, where the transportation noise is louder. The other routes are straighter and not aligned with the road. Following the roads is often a detour, which is time- and energy consuming, so this characteristic is unique for the least added noise flight routes.

The total flight distances in the height profiles (Fig. 4c, d) show, that the total travel distances of the least added noise routes are the longest of the three different objectives for both eVTOL types, even if the distances are marginally greater compared to the shortest flight time routes.

[1] https://www.esri.com/de-de/arcgis/products/arcgis-pro/resources
[2] https://www.python.org/downloads/release/python-368/

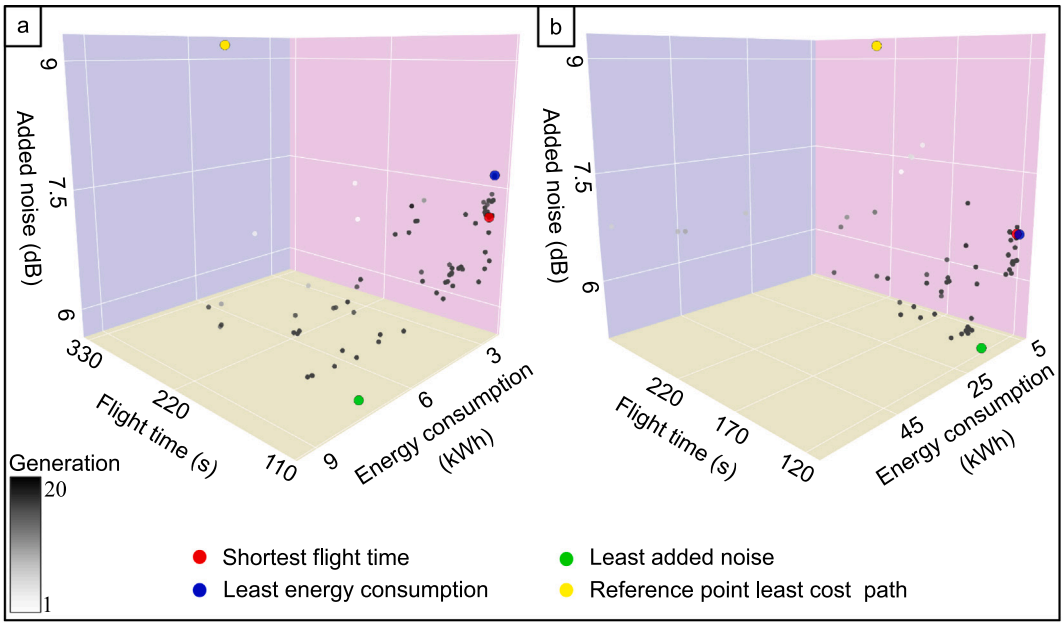

Fig. 3. Objective values of all generated non-dominated solutions in optimization, (a) aircraft EHANG 184, (b) Lilium jet. The grey-scale refers to the generation the solutions were produced. The extreme solutions for each objective are highlighted and the reference point of the least cost path is added. (For interpretation of the references to colour in this figure legend, the reader is referred to the web version of this article.)

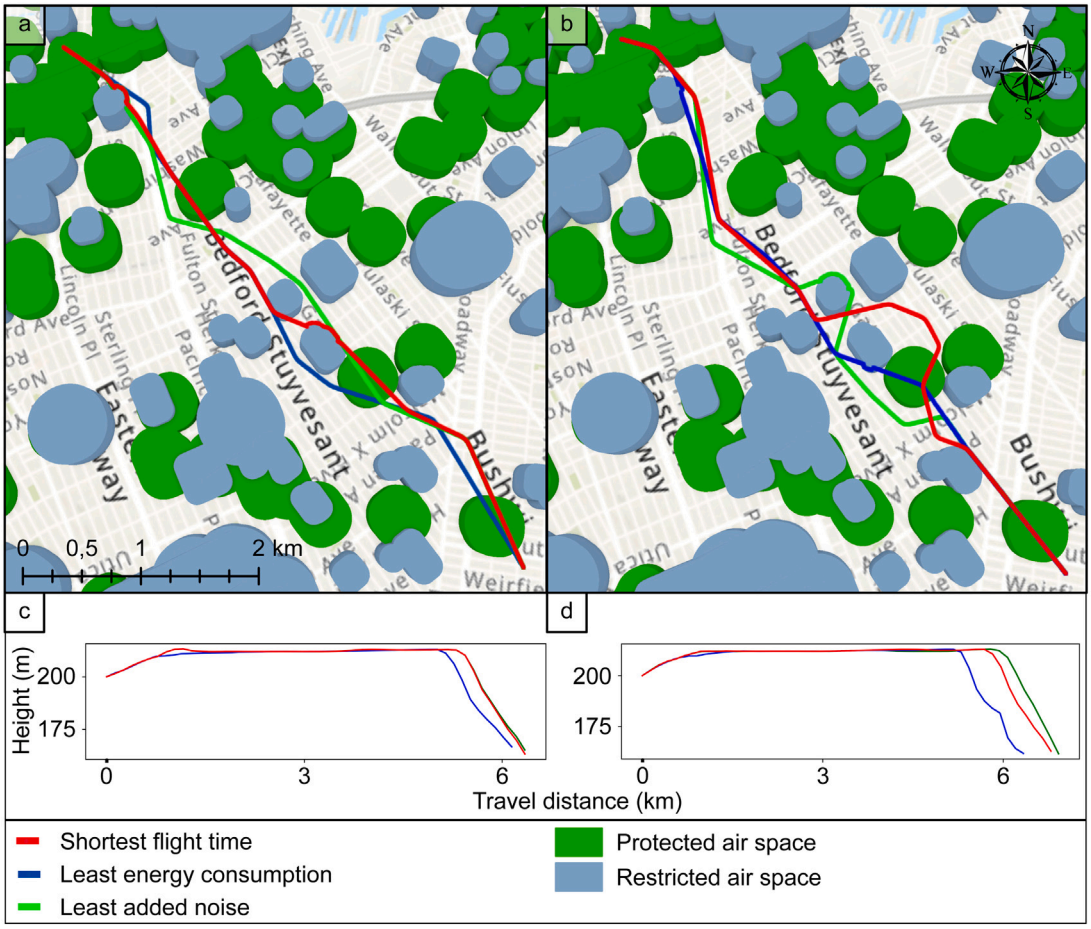

Fig. 4. Mapped 3D-routes for optimal solutions per objective, for eVTOL (a) EHANG 184 and (b) Lilium jet. The height profiles for all routes are illustrated for eVTOL (c) EHANG 184 and (d) Lilium jet.

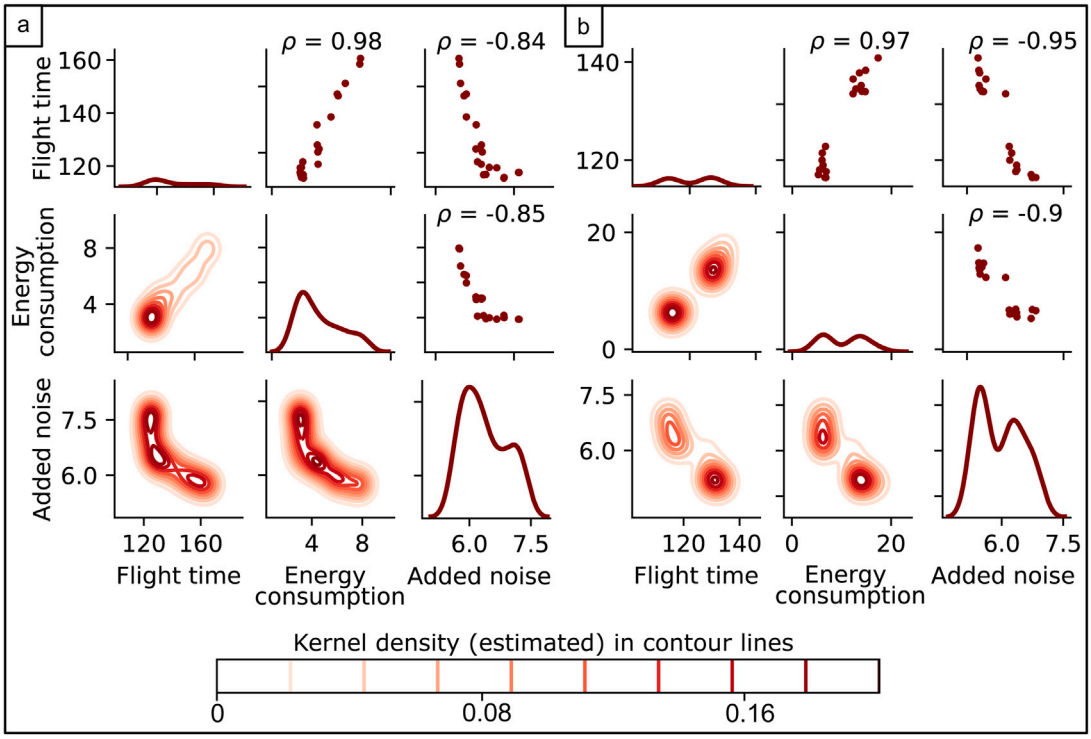

Fig. 5. Pairwise density distributions (diagonal), contour plots (lower-left) and scatter plots with correlation coefficients (upper-right) for all three objectives, for (a) the EHANG 184 and (b) the Lilium Jet.

4.2. Comparison of the extremes of the Pareto front with the least-cost path

The first part of the first research question "Can all objectives be optimized while complying with the air space restrictions and noise regulations?" can be answered with a yes. The best solutions, compared to the initial least cost path, were improved for both the EHANG 184 and the Lilium jet for all three objectives (Fig. 2). As this part can be answered with yes, the second part of the research question is addressed: How much can a least-distance route computed with a GIS be improved for the objectives in the highly restricted air space of New York City for two different eVTOL? Comparing the three extremes of the Pareto front to the least-cost path (Fig. 2), the flight time has decreased from 331 s to 115 s (65%), the energy consumption has decreased from 4.93 kWh to 2.38 kWh (52%), and the added noise has decreased from 9.19 dB to 5.74 dB (38%) for the EHANG 184. For the Lilium jet, the flight time has decreased from 220 s to 116.8 s (47%), the energy consumption has decreased from 9.99 kWh to 5.25 kWh (47%), and the added noise has decreased from 9.19 dB to 5.28 dB (43%). However, note that these three improvements cannot all be reached at the same time. In other words, there are trade-offs between the objectives.

4.3. Trade-offs between the three objectives

The energy consumption values of the Pareto front have a relatively narrow range for the EHANG 184 with values from 2.4 kWh to 12 kWh, compared to 5.3 kWh to 27 kWh for the Lilium jet. Similar behaviour can be observed for the objective shortest flight time. Only the value ranges for the added noise are similar between the aircraft types. As the optimization procedure is the same, this indicates a higher sensitivity to changes of the flight route structure for the Lilium jet: changes to the flight route structure of a certain magnitude have higher impacts on the route quality for the Lilium jet.

Our second research question was: What information is gained by the study case results? For both eVTOL aircraft types the energy consumption and the flight time of the optimal solutions are highly positively correlated, whereas the correlation coefficients of both of these objectives with added noise are highly negative (Fig. 5). This implies that lower added noise comes with longer flight times and more energy consumption. A linear regression of the final Pareto front shows that, on average, a decrease of 1 s of flight time comes with a reduction in energy consumption of 0.48 kWh for the Lilium jet and 0.1 kWh for the EHANG 184. A decrease of 1 kWh therefore comes with a decrease of 2.08 s flight time for the Lilium jet and 9.09 s for the EHANG 184. An increase in added noise of 1 dB comes with an additional flight time of 16 s for the Lilium jet and 26.9 s for the EHANG 184. In parallel to that, a decrease in flight time of one second comes with an additional noise of 0.06 dB for the Lilium and 0.037 dB for the EHANG 184. A decrease of 1 kWh of energy consumption comes with an additional noise level of 0.14 dB with the Lilium jet and 0.4 dB with the EHANG 184, which equals an additional 6.99 kWh (Lilium) and 2.48 kWh for every reduced noise level of 1 dB.

The reason for the positive correlation between the objectives energy consumption and flight time is the common component of the flight distance, which appears in the computation of both the flight time and energy consumption. In general, higher flight distances cause worse fitness values in energy and flight time together. On the other hand, the only distance in the objective function of the least added noise is the distance to the ground. A larger distance to the ground opposes short flight times and low energy consumption because the eVTOL is required to travel further.

The frequency distributions of non-dominated solutions differ per aircraft type (Fig. 5, panels at the diagonal). While the frequency distribution for the EHANG 184 is evenly spread, the non-dominated solutions for the Lilium jet are partitioned into two clusters (Fig. 5b). One cluster has high flight times, high energy consumption and low noise levels, the second cluster the opposite. There are no trade-off solutions in between these clusters, implying that there are no flight routes with medium performance for all three objectives.

The eVTOL characteristics in the objective functions explain these clusters. Sharp turns force both aircraft types to slow down, which increases the flight time. But, for the Lilium jet only, sharp turns also increase energy consumption. The Lilium Jet can produce lift

when travelling with higher flight speeds, which decreases energy consumption. The energy consumption in the hovering, acceleration and deceleration is higher than in cruise mode (Bacchini and Cestino, 2019). The energy consumption is therefore affected by route segments that have sharp turns, which forces the aircraft to shift from cruise mode to deceleration or hover mode. The required power increases from 36 to 187 kW, if the flight speed is 100 km/h. This does not apply to the multicoptor aircraft EHANG 184, as its energy consumption is the same in hover, acceleration, and deceleration. And with an increase in energy consumption from 34.6 to 42.7 kW, it is a smaller difference to shift from cruise mode to the other modes. Therefore, the EHANG 184 is not as affected by sharp turns along the route as the Lilium jet.

The flight routes that produce the lowest added noise follow the noisy parts of the city, which are mostly highly trafficked streets. Street networks in general tend to have many sharp turns. This also means that the best flight routes for the lowest added noise tend to have a higher negative impact on the lift-generating aircraft types than on the multicopter aircraft. These opposing requirements for good solutions for the different objectives explain the two observed clusters for the Lilium jet.

The same flight characteristics also explain, why the flight routes for the Lilium jet were observed to have higher value ranges in the objectives shortest flight time and least energy consumption (Fig. 4b). The initial points of the flight routes are random and have many sharp turns because connecting these random points leads to many sharp direction changes. Each of these turns has negative impacts on the objectives shortest flight time and least energy consumption. But, as discussed above, the negative impact is higher for lift-generating aircraft. The sharp turns are likely to be smoothed out from generation to generation because the idea of the evolutionary algorithm is to produce better children than the parents. The positive impacts of removing sharp turns are higher with the same reasoning. This sensitivity is also underlined by the higher improvement rates of optimizing the flight routes for the Lilium jet.

5. Discussion

5.1. Algorithm performance

In Section 4.1, it was shown that the algorithm managed to find better solutions than the least-cost path. The quality of the non-dominated solutions improved over the generations, and the improvements became smaller with each generation: The average improvements from the first to the second generation were 13.9% (Lilium) and 5.3% (EHANG), but only 1.4% (Lilium) and 0.0% (EHANG) in the last generation (Fig. 3). This is a sign of the desired outcome, that the solutions converge to an optimum. Furthermore, the number of non-dominated solutions increased over time. The last generation contained on average 220% more non-dominated solutions than the first generation. The more non-dominated solutions are produced, the better we can derive the shape of the Pareto front, and the more options the decision maker has for the selection of a single solution (Deb and Chaudhuri, 2007). The convergence behaviour of the evolutionary algorithm was found to differ per aircraft, with smaller improvements per generation for the EHANG (Fig. 3).

The relative flight route quality improvement in the objective of least added noise was lower compared to the relative quality improvement in the other two objectives for both aircraft types. This can be explained by the difference in the solution-space complexity for each objective, which we have illustrated with an example in Fig. 6. For an easier understanding, we remove the height dimension from the objective functions and only consider two-dimensional position changes. For the energy and flight time, the positions that improve the fitness, because the course of the flight route straightens (green marked area), are close to the current position of the point and clustered together. On the other hand, positions that improve the minimal added noise are more difficult to find, because they are far away from the current position, not clustered, and in different directions from the current position. The best position for the lowest added noise is the corner at the bottom right of Fig. 6. The best approach to get to this solution would be a totally random positioning, so the solution can only be found by chance. An adaptation for making the search easier to find the noisy areas can be done by smoothing the input noise data. Filtering processes, for example a Gaussian smoothing (Longley et al., 2015), can cause the raster file to produce a more continuous search space, but at the same time this would make the detected solutions less precise.

5.2. Implications for air space management

If a goal of air space management is that the yearly average background noise change shall not increase by more than 1 dB (Uber Elevate, 2016; Berglund et al., 1999) (because this the smallest change that can be detected by a person), our results show that this goal cannot be reached. The added noise we computed, even for the route with the lowest added noise at the extreme of the Pareto front, has an average added noise of ≈ 5 dB. A potential solution would be vary the route over the course of the day, adapting it to traffic, or to select a less noisy aircraft than the ones evaluated in this work. It is also advisable, to make the objective noise more important for flight routes meant for night-time flights and possibly to include residential areas into the no-fly zones at night.

One important consideration in our method with respect to flight management is the level of detail of the flight route representation. The result of our current optimization is a 3D-line with an accuracy of less than a centimetre. But in reality, aircraft are not able to follow the line with such precision, even if the maximum speeds are preserved. Wind gusts or minor piloting errors, just as two examples, can lead to a misallocation of the aircraft from the flight route. Therefore, if this work is to be used for air space management it is advisable to compute the objective values on 3D pipes around the flight route lines. One possibility for this transformation is adding three different boundaries around the line, which can be equivalent to a geofence safety boundary management developed by NASA (Dill et al., 2016).

5.3. Generalizability and limitations

In this study, we focus on computing flight routes for air taxis only. However, other airspace users than air taxis will populate the urban airspace e.g. drones operating in the lower airspace (Merkert and Bushell, 2020). This yields the risk of collisions and airspace congestion. For this reason, airspace management systems will be required that manage the operations of all airspace users. A solution to control all airspace operations is a variable pricing strategy for the different airspace users (Merkert et al., 2021). For temporal permissions to access specific flight corridors, variable charges can be utilized that may consider various factors. Such factors can be, for example, the aircraft type, the maximum speed, the demand for operating at the desired flight height, but also externalities such as added noise or added risk. The variable charges can be considered in flight route planning by defining an alternative objective function that quantifies the total charges per air taxi operation. Since some factors change over time, e.g. the demand or the added noise, this strategy would result in temporally changing optimal flight routes. A flight route optimization that considers all airspace users yields many challenges and thus potential for future research.

In this work, the objective functions are approximations of the real flight time, energy consumption, and added noise. We considered the added noise directly underneath the aircraft's position. In future work, the added noise to the neighbouring areas could be computed too. Furthermore, it is not clear how noisy the aircraft are in reality, because the air-taxi manufacturers did not supply any information about the

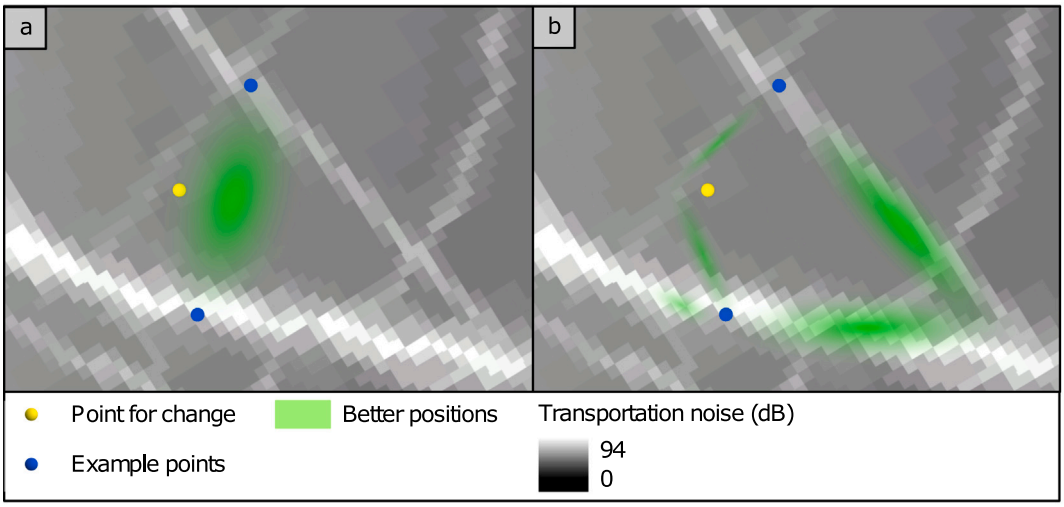

Fig. 6. Illustration of solution-space complexity. Green area displays regions of better positions compared to the current yellow point for (a) the objectives least energy consumption and shortest flight time, and (b) the objective least added noise. (For interpretation of the references to colour in this figure legend, the reader is referred to the web version of this article.)

sound pressures or about the sound frequencies. This is a limitation that cannot be solved without the cooperation of the manufacturers.

Besides, the impact of wind can be considered. Depending on the wind direction and wind speed, the wind conditions can change rapidly and can be distributed unevenly in the city area (Bornstein and Johnson, 1977). High wind speeds from specific directions can lead to differences in energy consumption for different flight directions, unequal propagation of noise, as well as in dangerous areas, which would need to be modelled in time-dependent no-fly zones (Stevens and Atkins, 2019; Geister, 2017).

The origin and destination chosen in Manhattan, New York, was one of many possible ones. To demonstrate the robustness of our results, we selected a second origin–destination pair, computed a second least-cost path with a length of 18 km, and redid the optimization. The results are displayed in Appendix D (Fig. 8 and Fig. 9). For any different path in the same study area, only the input least-cost path needs to be changed. For the application of 3D-flight route optimization in a different study area, the method is generally applicable if the data requirements are met. Information to compute the restricted flight areas needs to be available, as well as the surface with the minimal flight height. Suppose the flight route optimization is intended to be applied to different aircraft. In that case, the only required adaptation is to alter the aircraft specifications.

6. Conclusion

In this work, we proposed a 3D-route optimization method with novel GIS procedures like seeding and repair. The method was applied to a case study in Manhattan in New York for two different eVTOL Lilium Jet and EHANG 184. The proposed method is also applicable to other urban areas, different aircraft types and other 3D-routing applications.

Our first research question was: Can all objectives be optimized while complying with the air space restrictions and noise regulations? If yes, how much can least distance flight routes computed with a GIS be improved for multiple objectives in the highly restricted air space of New York City for two different eVTOL? Our results confirmed the first part of this question. Compared to the least cost path (Fig. 2), the flight time has decreased by 65% from 331 s to 115 s, the energy consumption by 52% from 4.93 kWh to 2.38 kWh, and the added noise decreased by 38% from 9.19 dB to 5.74 dB for the EHANG 184. For the Lilium jet, the flight time has decreased by 47% from 220 s to 116.8 s, the energy consumption by 47% from 9.99 kWh to 5.25 kWh, and the added noise decreased by 43% from 9.19 dB to 5.28 dB.

Our second research question was: What information for air space management can be derived from the study case results? The produced non-dominated solutions showed high positive correlations between the objectives flight time and energy consumption, while they are both highly negatively correlated to the objective of least added noise. One lesson learned was that lift-generating aircraft are more sensitive to the flight route characteristics, such as bends, while more trade-off solutions exist for multicoptor aircraft. Another information gain regards the hardness of finding an optimum for the objective of least added noise. It is easier to find better solutions for lower energy consumption and shorter flight times because the fitness landscape is smoother with fewer local optima.

Another thing we can conclude is that without changing the flight routes over time it is not possible to comply with the noise regulations not to increase the long-term noise by more than 1 dB. The average noise additions were more than 5 dB, which is considered an unacceptable long-term annoyance.

CRediT authorship contribution statement

Moritz Hildemann: Conceptualization, Methodology, Software, Writing – original draft, Visualization. **Judith A. Verstegen:** Supervision, Conceptualization, Methodology, Writing – review & editing.

Declaration of competing interest

The authors declare that they have no known competing financial interests or personal relationships that could have appeared to influence the work reported in this paper.

Appendix A. Repair geo-processes

If a 3D-point lies within a restricted or protected air space, additional reference points are created before the optimization process begins. The reference points were created in 10-meter distance from the border lines of the restricted or protected air space. All 3D-points, that are positioned in the restricted air space, are relocated to the x- and y-coordinate of the nearest reference point as illustrated in Fig. 7 (left). The line repair function repairs intersections of 3D-lines with the restricted airspace. Even if the 3D-points are not positioned in the 3-dimensional restricted or protected air space after the point relocation,

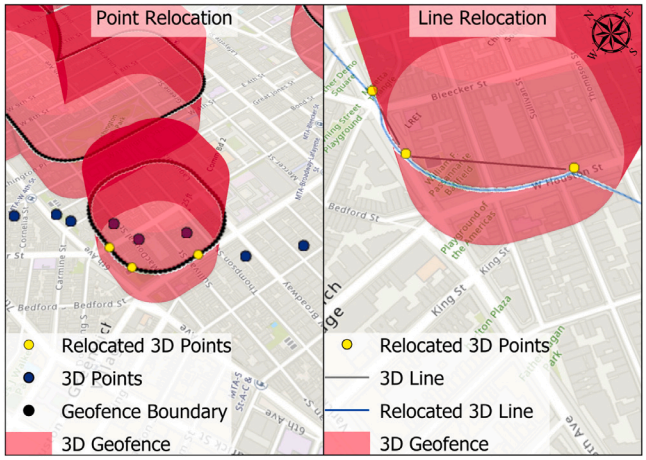

Fig. 7. Illustration of repairing points and lines intersecting with restricted or protected air spaces.

the connecting line segments might do intersect with the restricted air space, as can be seen in Fig. 7 (right).

At first, the intersection points of the 3-line with the 3D-shape are computed. From these intersection points, the nearest two neighbouring points from the restricted or protected air space point boundary are added to two arrays. For each point, the nearest neighbour will be added to the array. Now, for every last point of each array, the nearest neighbour point that does not yet exist in any of the two arrays is added. This procedure is repeated until the second intersection point is added to one of the two arrays. The points in the arrays are inserted into the point representation. In this way, the restricted or protected air space is surrounded in both directions and the shorter way is used to be inserted to the point representation. If the 3D-point representation is now converted to a line again by connecting the points, the line is not intersecting with the restricted or protected air space anymore. The repaired line is illustrated in Fig. 7 (right, Relocated 3D-Line). In order to achieve this point-to-line conversion without crossings, the points need to be in the correct order. This is achieved by reordering all 3D-points after all point and line repairs, from the starting point to the end node. After this, the old 3D-line representation is replaced by the repaired 3D-lines. All changes are propagated to all three representations of the solution.

Algorithm 1 Line repair

```
[RoutePoints] = [Points]                                   ▷ Points of flight route
ip1, ip2 ← Intersect(FlightRoute, RestrictedorProtectedAirspace)   ▷ Intersection points
bp1, bp2 ← Near(ip1, PointBoundary)                        ▷ Two nearest boundary points
[way1], [way2] ← [Points]                                  ▷ Initialize empty arrays
while ip2 ∉ [way1, way2] do                                ▷ Stops if the second intersection point is reached
    np1 ← Near(bp1)
    if np1 ∉ [way1, way2] then
        b1 ← np1
        [way1].add(bp1)
    end if
    np2 ← Near(bp2)
    if np2 ∉ [way1, way2] then
        b2 ← np2
        [way2].add(bp2)
    end if
    if [way1].last = ip2 then
        [Route].add([way1])
    end if
    if [way2].last = ip2 then
        [RoutePoints].add([way2])
    end if
end while
[RoutePoints] ← Reorder([RoutePoints])
Line ← PointsToLine([RoutePoints])
return [RoutePoints], Line                                 ▷ Returns flight route with new elements
```

Appendix B. Cost function computations

B.1. Maximum flight speed

To compute the maximum flight speed, the maximum flight speed for each position is computed with its centripetal forces. As the flight route is no single circle, the centripetal force changes at each point of the route. In order to compute the centripetal acceleration at each position, an imaginary circle is computed. This imaginary circle is constructed at every point with its two neighbour points. The radius of the imaginary circle is used to compute the centripetal acceleration a_c and the resulting maximal velocity v_{max} for the maximum g_{Force} of 1.25. The formulas for the computation are expressed in Eqs. (1)–(3).

$$a_c = \frac{v^2}{r} \tag{1}$$

$$g_{Force} = \frac{a_c}{g_m} \tag{2}$$

$$v_{max} = \sqrt{g_{ForceMax} \cdot r \cdot g_m} \tag{3}$$

where

a_c	Centripetal acceleration in $\frac{\mathrm{m}}{\mathrm{s}^2}$
v	Velocity in $\frac{\mathrm{m}}{\mathrm{s}}$
r	Circle radius in m
g_{Force}	Gravitational force equivalent
$g_{ForceMax}$	Maximum allowed g-force
g_m	Gravitational acceleration of $9.81\frac{\mathrm{m}}{\mathrm{s}^2}$
v_{max}	Maximum allowed speed at the given radius and maximum g-force

The output is the maximal flight speed at each position, which is the minimum value of the maximal allowed legal flight speed, the maximum speed of the aircraft and the maximum speed to have a lower g_{Force} than 1.25.

B.2. Flight time computation

The total flight time with the specified flight constraints is the added-up flight time of all line segments:

$$t_{total} = \sum_{i=1}^{n} \frac{d_i}{v_i} \tag{4}$$

where

t_{total}	Total flight time
n	Number of line segments
d_i	Euclidean distance from the current point to next point
v_i	Flight velocity at current segment

To calculate the flight time of each segment, we use the distances between the points and actual flight speeds. If the aircraft is slower than the allowed flight speed at the next position, the aircraft accelerates with $2\frac{\mathrm{m}}{\mathrm{s}^2}$. If the allowed flight speed of the next position is lower than the current flight speed, the aircraft decelerates with $-2\frac{\mathrm{m}}{\mathrm{s}^2}$. Furthermore, it needs to be assured, that the distance to the next point

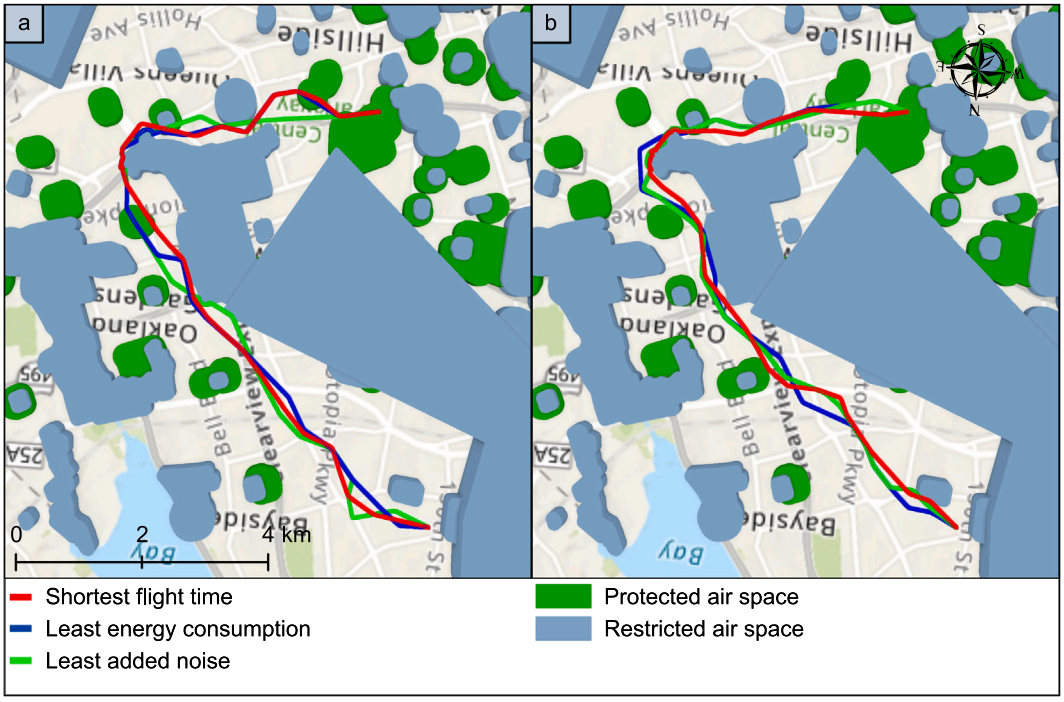

Fig. 8. Mapped 3D-routes for optimal solutions per objective, for eVTOL (a) EHANG 184 and (b) Lilium jet.

is sufficiently big in order to decelerate to the allowed flight speed. If the distance is not long enough, the flight speeds of the previous points are readjusted.

B.3. Energy consumption computation

Now, with the variables flight velocity and the flight angle, the required power can be calculated for each flight route segment by following the calculus of Eq. (5)–(11) (Sadraey, 2009). The velocity is derived from the previous step and the ascending/descending angle is computed for each point to the next point. By summing up the required power of all segments, the desired objective function for getting the total energy consumption in kWh is complete (Eq. (12)).

$$L_C = W * cos(\gamma) \tag{5}$$

$$L_{CL} = \frac{L_C}{\frac{1}{2}p^2 S} \tag{6}$$

$$C_{DC} = C_{D0} + K * C_L^2 \tag{7}$$

$$D_C = \frac{1}{2} p V^2 S C_{DC} \tag{8}$$

$$T_{RC} = W \sin(\gamma) + D_C \tag{9}$$

$$T_{RC} = W \sin(\gamma) + D_C \tag{10}$$

$$P_{RC} = \frac{T_{RC}}{1000} \tag{11}$$

$$P_{RC_{total}} = \sum_{i=1}^{n} P_{RC_i} * \frac{d_i}{v_i} \tag{12}$$

where

L_C	Required lift
W	Weight of aeroplane in N
γ	Angle of climb/descent in °
L_{CL}	Lift coefficient in climb
S	Wing area of aircraft in m^2
V	Flight speed in $\frac{m}{s}$
p	Min. Air density $\frac{kg}{m^3}$
C_{DC}	Drag coefficient in climb
K_C	Drag factor
C_{D0}	Total zero-lift drag
D_C	Drag in climb in N
T_{RC}	Thrust required in N
P_{RC}	Power required in climb in kW
$P_{RC_{total}}$	Total required power of flight route
n	Number of line segments
d_i	Euclidean distance from current line segment i
v_i	Flight velocity at current segment i

B.4. Noise addition computation

The first step is to calculate the sound pressure arriving at the ground (Kinsler, 2000). For this calculation, the noise emission of the aircraft is required. These values are not made public by the aircraft manufacturers, therefore the targeted noise level of Uber Elevate is used as a replacement. Uber Elevate (2016) is the only available source to mention the noise level targets. Their goal is a maximum of "62 dB at 500 ft altitude". This translates to a noise pressure of 100 dB in a reference distance of one meter. By filling the variable r in Eq. (13) with the current flight height we get the perceived noise level at ground from the aircraft.

The next step is to combine the noise emission by the aircraft with the background noise on the ground. The used data for the background noise is the average daily sound level from aviation and interstate road noise. The data was made available by the U.S. Department of Transportation (Bureau of Transportation Statistics, 2014). By combining the aircraft and background noise by inserting corresponding noise levels at variable $L_{P,i}$ in Eq. (14), the total noise level $L_{P.Tot}$ is computed. At this point, it is possible to determine how much noise the aircraft

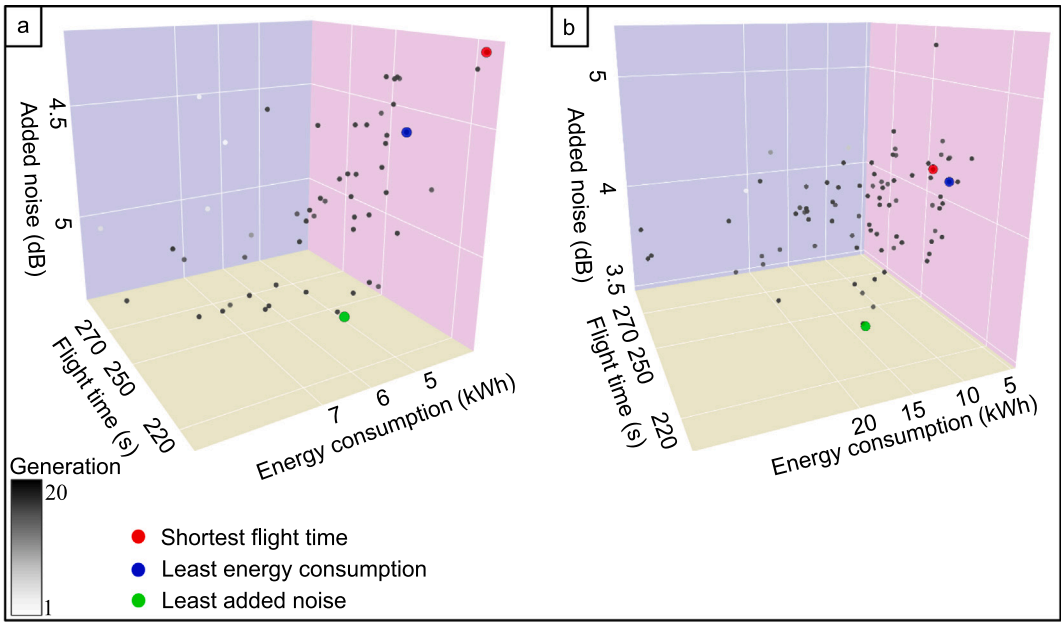

Fig. 9. Convergence behaviour, for eVTOL (a) EHANG 184 and (b) Lilium jet.

added at ground (Eq. (15)). In this equation can be observed, that the noise addition is higher if the background noise is lower. Therefore, the proposed objective function complies with the idea of preferring areas with a high background noise.

$$L_P = L_m - 20\log_{10}\frac{r}{r_m} \tag{13}$$

$$L_{P.Tot} = 10\log\left(\sum_i 10^{0.1L_{P.i}}\right) \tag{14}$$

$$L_{P.Source} = 10\log\left(10^{0.1L_{P.Total}} - 10^{0.1L_{P.Background}}\right) \tag{15}$$

where

L_P	Sound pressure at the ground[a]
r	Distance to ground
r_m	Reference distance (1 m from aircraft)
L_m	Sound level at reference distance (100 dB)
$L_{P.i}$	Each noise from source i measured at ground
$L_{P.Tot}$	Combined noise pressure from background and aircraft noise
$L_{P.Source}$	Added noise pressure from aircraft at ground

[a]All sound pressure units are expressed in *decibel* (dB).

The average added noise level is calculated by averaging all added noise levels at each point at the flight route.

Appendix C. Adaptation of the n-point crossover

1. The N randomly chosen positions are chosen in a range between 1 and the length of the shorter parent −1. The last position and first position are not exchanged as they are always the starting and ending point of the flight route.
2. For each recombination point N of the first parent, the nearest flight route point of the second parent is sought with a GIS Near Point Analysis from ArcGIS Pro. These points are the beginning points of the point exchanges.
3. With both recombination positions of the parents, the children are produced by exchanging the parent segments. Up to the first recombination point, children 1 gets the segments of parent 1, and children 2 gets the segments of parent 1. After the first recombination point children 1 gets the segments of parent 2 and children 2 gets the segments of parent 2. This changes at each recombination point N.
4. The points of the children are reordered. All changes are propagated to the array, point and line representations.

Appendix D. Evaluation of a second origin–destination pair

See Figs. 8 and 9.

References

Ahmed, S.S., Fountas, G., Eker, U., Still, S.E., Anastasopoulos, P.C., 2021. An exploratory empirical analysis of willingness to hire and pay for flying taxis and shared flying car services. J. Air Transp. Manag. 90, 101963. http://dx.doi.org/10.1016/j.jairtraman.2020.101963.

Atila, U., Karas, I., Rahman, A., 2013. A 3D-GIS implementation for realizing 3D network analysis and routing simulation for evacuation purpose. In: Pouliot, J., Daniel, S., Hubert, F., Zamyadi, A. (Eds.), Progress and New Trends in 3D Geoinformation Sciences. In: Lecture Notes in Geoinformation and Cartography, vol. 29, Springer Berlin Heidelberg, Berlin, Heidelberg, pp. 249–260. http://dx.doi.org/10.1007/978-3-642-29793-9-14.

Bacchini, A., Cestino, E., 2019. Electric VTOL configurations comparison. Aerospace 6 (3), 26. http://dx.doi.org/10.3390/aerospace6030026.

Baur, S., Schickram, S., Homolenko, A., Martinez, N., Dyskin, A., 2018. In: Roland Berger (Ed.), Urban Air Mobility: The Rise of a New Mode of Transportation. In: Focus, URL: https://www.rolandberger.com/publications/publication_pdf/Roland_Berger_Urban_Air_Mobility.pdf.

Bauranov, A., Rakas, J., 2021. Designing airspace for urban air mobility: A review of concepts and approaches. Prog. Aerosp. Sci. 125, 100726. http://dx.doi.org/10.1016/j.paerosci.2021.100726.

Berglund, B., Lindvall, T., Schwela, D., 1999. Guidelines for Community Noise. Stockholm University.

Bornstein, R.D., Johnson, D.S., 1977. Urban-rural wind velocity differences. Atmos. Environ. (1967) 11 (7), 597–604. http://dx.doi.org/10.1016/0004-6981(77)90112-3.

Budde, D., Hinkelbein, J., Boyd, D.D., 2021. Analysis of air taxi accidents (20042018) and associated human factors by aircraft performance class. Aerosp. Med. Hum. Perform. 92 (5), 294–302. http://dx.doi.org/10.3357/AMHP.5799.2021.

Bureau of Transportation Statistics, 2014. National transportation noise map. URL: https://www.bts.gov/newsroom/bts-releases-national-transportation-noise-map.

Dai, W., Low, K.H., 2022. Conflict-free trajectory planning for urban air mobility based on an airspace-resource-centric approach. In: AIAA Aviation 2022 Forum. American Institute of Aeronautics and Astronautics, Reston, Virginia, http://dx.doi.org/10.2514/6.2022-4077.

de Paiva Vianna, K.M., Cardoso, M.R.A., Rodrigues, R.M.C., 2015. Noise pollution and annoyance: an urban soundscapes study. Noise & Health 17 (76), 125–133. http://dx.doi.org/10.4103/1463-1741.155833.

Deb, K., Chaudhuri, S., 2007. I-MODE: An interactive multi-objective optimization and decision-making using evolutionary methods. In: Obayashi, S., Deb, K., Poloni, C., Hiroyasu, T., Murata, T. (Eds.), Evolutionary Multi-Criterion Optimization. In: Lecture Notes in Computer Science, vol. 4403, Springer Berlin Heidelberg, Berlin, Heidelberg, pp. 788–802. http://dx.doi.org/10.1007/978-3-540-70928-2_59.

Deb, K., Pratap, A., Agarwal, S., Meyarivan, T., 2002. A fast and elitist multiobjective genetic algorithm: NSGA-II. IEEE Trans. Evol. Comput. 6 (2), 182–197. http://dx.doi.org/10.1109/4235.996017.

Dill, E.T., Young, S.D., Hayhurst, K.J. (Eds.), 2016. SAFEGUARD: An assured safety net technology for UAS, thirty fifth ed. DASC, In: 2016 IEEE/AIAA 35th Digital Avionics Systems Conference, IEEEC, http://dx.doi.org/10.1109/DASC.2016.7778009.

Durmaz, A., Ünal, E., Aydın, C., 2019. Automatic pipeline route design with multi-criteria evaluation based on least-cost path analysis and line-based cartographic simplification: A case study of the mus project in Turkey. ISPRS Int. J. Geo-Inf. 8 (4), 173. http://dx.doi.org/10.3390/ijgi8040173.

EHANG, 2019. Ehang 184 specifications. URL: http://www.ehang.com/ehang184/specs.

Eißfeldt, H., 2020. Sustainable urban air mobility supported with participatory noise sensing. Sustainability 12 (8), 3320. http://dx.doi.org/10.3390/su12083320.

Electric VTOL News, 2019. Evtol Classifications. World eVTOL Directory, URL: https://evtol.news/classifications/.

Environmental Protection Agency, 1974. Information on levels of environmental noise requisite to protect public health and welfare with an adequate margin of safety: EPA: U.S. URL: http://www.nonoise.org/library/levels74/levels74.htm.

Federal Aviation Administration, 2017. Pilot's Handbook of Aeronautical Knowledge: 2016, First Skyhorse Publishing ed. Skyhorse Publishing, New York, NY.

Federal Flight Administration, 2016. Digital obstacle file: Flight obstacle maps. URL: https://www.faa.gov/air_traffic/flight_info/aeronav/digital_products/dof/.

Friedrich, T., Wagner, M., 2015. Seeding the initial population of multi-objective evolutionary algorithms: A computational study. Appl. Soft Comput. 33, 223–230. http://dx.doi.org/10.1016/j.asoc.2015.04.043.

Garrow, L.A., German, B.J., Leonard, C.E., 2021. Urban air mobility: A comprehensive review and comparative analysis with autonomous and electric ground transportation for informing future research. Transp. Res. C 132, 103377. http://dx.doi.org/10.1016/j.trc.2021.103377.

Geister, D., 2017. Integrating UAS into the Future Aviation System: A Flexible Approach Enabling Large-Scale UAS Operations: German Aerospace Center (DLR). Institute of Flight Guidance, URL: http://www.dlr.de/fl/desktopdefault.aspx/tabid-11763/20624_read-48305/.

Glaab, P., Wieland, F., Santos, M., Sharma, R., Tamburro, R., Lee, P.U., 2019. Simulating fleet noise for notional UAM vehicles and operations in New York. In: 2019 IEEE/AIAA 38th Digital Avionics Systems Conference. DASC, IEEE, pp. 1–10. http://dx.doi.org/10.1109/DASC43569.2019.9081670.

Goyal, R., 2018. Urban Air Mobility (UAM) market study: Presented to: National Aeronautics and Space Administration - Aeronautics Research Mission Directorate. In: Booz-Allen and Hamilton, Inc. (Ed.), In: Air Transportation and Safety, NASA Headquarters and Washington, DC, United States, URL: https://ntrs.nasa.gov/search.jsp?R=20190001472.

Hildemann, M., 2020. 3D flight route optimization for air-taxis in urban areas (Python + arcpy repository), Mendeley Data, http://dx.doi.org/10.17632/kzk3j8xhhm.1, https://data.mendeley.com/datasets/kzk3j8xhhm.

Hildemann, M., Delgado, C., 2019. An adaptable and scalable least cost network for air-taxis in urban areas study area: Manhattan, New York. In: Accepted Short Papers and Posters from the 22nd AGILE Conference on Geo-Information Science. AGILE.

Hildemann, M., Delgado, C., 2020. Spatial input data for computing air-taxi flight routes in restricted and protected air spaces in New Yerk City (USA). http://dx.doi.org/10.17632/b3n53j747h.1.

Holland, J.H., 1975. Adaptation in Natural and Artificial Systems: An Introductory Analysis with Applications to Biology, Control, and Artificial Intelligence. University of Michigan Press, Ann Arbor, Michigan.

Kinsler, L.E., 2000. Fundamentals of Acoustics, fourth ed. Wiley, New York and Chichester, URL: https://www.who.int/occupational_health/publications/noise1.pdf.

Lilium Aviation, 2019. Mission: Aircraft for everyone. URL: https://lilium.com/mission/.

Longley, P., Goodchild, M.F., Maguire, D., Rhind, D.W., 2015. Geographic Information Science & Systems, fourth ed. John Wiley & Sons, Hoboken, New Jersey.

McKinsey & Company, 2021. Study on the societal acceptance of urban air mobility in Europe. URL: https://www.easa.europa.eu/sites/default/files/dfu/uam-full-report.pdf.

Merkert, R., Beck, M.J., Bushell, J., 2021. Will it fly? Adoption of the road pricing framework to manage drone use of airspace. Transp. Res. A 150, 156–170. http://dx.doi.org/10.1016/j.tra.2021.06.001.

Merkert, R., Bushell, J., 2020. Managing the drone revolution: A systematic literature review into the current use of airborne drones and future strategic directions for their effective control. J. Air Transp. Manag. 89, 101929. http://dx.doi.org/10.1016/j.jairtraman.2020.101929.

Okuniek, J.N., Gerdes, I., Jakobi, J., Ludwig, T., Hooey, B.L., Foyle, D., Jung, Y.C., Zhu, Z., 2016. A concept of operations for trajectory-based taxi operations. In: 16th AIAA Aviation Technology 2016. http://dx.doi.org/10.2514/6.2016-3753.

Open Data NYC, 2018. Open data of New York City: New York City population by neighborhood tabulation areas. In: NYC.gov (Ed.), New York, URL: https://opendata.cityofnewyork.us/.

OpenStreetMap contributors, 2019. https://planet.osm.org. URL: https://www.openstreetmap.org.

Peng, Z., Wu, J., Chen, J., 2011. Three-dimensional multi-constraint route planning of unmanned aerial vehicle low-altitude penetration based on coevolutionary multi-agent genetic algorithm. J. Cent. South Univ. Technol. 18 (5), 1502–1508. http://dx.doi.org/10.1007/s11771-011-0866-4.

Pradeep, P., Chatterji, G.B., Lauderdale, T.A., Sheth, K., Lai, C.F., Erzberger, H., Sridhar, B., 2022. Wind-optimal lateral trajectories for a multirotor aircraft in urban air mobility. Front. Aerosp. Eng. 1, http://dx.doi.org/10.3389/fpace.2022.1064142.

Pradeep, P., Lauderdale, T.A., Chatterji, G.B., Sheth, K., Lai, C.F., Sridhar, B., Edholm, K., Erzberger, H., 2020. Wind-optimal trajectories for multirotor eVTOL aircraft on UAM missions. In: AIAA Aviation Forum 2020. http://dx.doi.org/10.2514/6.2020-3271.

Rajendran, S., Pagel, E., 2020. Recommendations for emerging air taxi network operations based on online review analysis of helicopter services. Heliyon 6 (12), e05581. http://dx.doi.org/10.1016/j.heliyon.2020.e05581.

Rajendran, S., Srinivas, S., 2020. Air taxi service for urban mobility: A critical review of recent developments, future challenges, and opportunities. Transp. Res. E 143, 102090. http://dx.doi.org/10.1016/j.tre.2020.102090.

Reddy, M.J., Kumar, D.N., 2015. Elitist-mutated multi-objective particle swarm optimization for engineering design. In: Khosrow-Pour, D.B.A. (Ed.), Encyclopedia of Information Science and Technology, third ed. IGI Global, pp. 3534–3545. http://dx.doi.org/10.4018/978-1-4666-5888-2.ch346.

Rizzi, S.A., Huff, D.L., Boyd, D.D., Bent, P., Henderson, B.S., Pascioni, K.A., Sargent, D.C., Josephson, D.L., Marsan, M., He, H.B., Snider, R., 2020. Urban air mobility noise: Current practice,gaps, and recommendations. NASA Sci. Tech. Inf. (STI).

Sadraey, M., 2009. Aircraft Performance Analysis. VDM Verlag Dr. Müller, Saarbrücken, Germany.

Sandurkar, S., Chen, W., 1999. GAPRUS - genetic algorithms based pipe routing using tessellated objects. Comput. Ind. 38 (3), 209–223. http://dx.doi.org/10.1016/S0166-3615(98)00130-4.

Sivanandam, S., Deepa, S., 2008. Introduction to Genetic Algorithms. Springer, Berlin.

Stevens, M.N., Atkins, E.M., 2019. Generating airspace geofence boundary layers in wind. J. Aerosp. Inf. Syst. 1–12. http://dx.doi.org/10.2514/1.I010792.

Sun, X., Wandelt, S., Stumpf, E., 2018. Competitiveness of on-demand air taxis regarding door-to-door travel time: A race through Europe. Transp. Res. E 119, 1–18. http://dx.doi.org/10.1016/j.tre.2018.09.006.

Uber Elevate, 2016. Fast-forwarding to a future of on-demand urban air transportation: White paper. URL: https://www.uber.com/us/en/elevate/.

Wang, M., Diepolder, J., Zhang, S., Söpper, M., Holzapfel, F., 2021. Trajectory optimization-based maneuverability assessment of eVTOL aircraft. Aerosp. Sci. Technol. 117, 106903. http://dx.doi.org/10.1016/j.ast.2021.106903.

Ward, K.A., Winter, S.R., Cross, D.S., Robbins, J.M., Mehta, R., Doherty, S., Rice, S., 2021. Safety systems, culture, and willingness to fly in autonomous air taxis: A multi-study and mediation analysis. J. Air Transp. Manag. 91, 101975. http://dx.doi.org/10.1016/j.jairtraman.2020.101975.

Zhao, N., Li, N., Sun, Y., Gao, Z., 2020. 4D trajectory planning of aircraft taxiing considering time and fuel. Math. Probl. Eng. 2020, 1–12. http://dx.doi.org/10.1155/2020/9603968.